(Received 28 January 2024, Accepted 4 March 2024, Scheduled 15 March 2024)

Microstrip Patch Antenna with Multi-Fins for Radio Frequency Energy Harvesting Applications

Mohammed M. Hasan* and Ahmed M. A. Sabaawi

Electronic Engineering Department, College of Electronics Engineering, Ninevah University, Mosul, Iraq

ABSTRACT: A novel multiband microstrip patch antenna (Antenna-1) is introduced in this paper to target the frequencies of interest required for RF energy harvesting applications, including mobile DCS (Digital Cellular System), mobile LTE (Long Term Evolution), mobile 5G, WLAN (Wireless Local Area Network), and WIMAX (Worldwide Interoperability for Microwave Access) services. The simulated results for the proposed antenna showed outstanding performance. The antenna supports a high number of total (11) eleven operating frequencies and covers all of the frequencies of the 2.4 GHz (IEEE 802.11) band, as well as the downlink frequencies of mobile DCS 1800 and the downlink frequencies for mobile LTE/5G (Band 68). The proposed antenna has achieved a high gain for most of its resonating frequencies, with a high gain of (4.49 dBi) at the frequency of (2.4527 GHz) and a peak gain of (6.349 dBi) at the frequency of (3.95 GHz). Furthermore, the proposed antenna achieved a high bandwidth capacity of (677 MHz) at the resonating frequency of (5.2 GHz), which covers a lot of frequencies utilized by WLAN, WIMAX, and mobile LTE services, making it a suitable antenna for radio frequency energy harvesting applications. Good agreement between the measured and simulation results was observed.

1. INTRODUCTION

Radio Frequency Energy Harvesting (RFEH) has come to be regarded as a desirable method of employing ambient radio frequency signals to power low-power electronic devices since a lot of research has been done to improve the performance of RF energy-harvesting systems and may offer reliable and sustainable power sources for low-power electronic equipment in the future. The Internet of Things (IoT) is developing quickly and has brought a vast number of sensors and connected devices to the internet, and by 2025, there will be over 30.9 billion connected devices [1]. One of the key elements of the Internet of Things (IOT) is sensor networks, which include wired and wireless sensors (WSs). These networks exchange environmental data in real-time, such as temperature, light, and humidity, and use that data to preserve the ecosystem and ensure user fulfillment. WSs can be installed in inaccessible places like chemical production facilities, the ocean's depths, disaster-prone areas, agricultural farms, and subterranean locations, and they have become more popular than wired sensors. Researchers have been looking into a number of energies harvesting techniques to reduce maintenance costs and enable low-power devices such as wireless sensors that are placed remotely to operate on their own since these wireless sensors' batteries must be changed frequently in order to prolong the duration of their use [2]. The impedance matching network, rectification circuit, power management unit, and receiving antenna are the main elements of the radio frequency energy harvesting system. The receiving antenna plays a crucial role in the functioning of the RFEH system because it is in charge of gathering ambient radio frequency energy from the free space and converting it to a usable DC voltage by connecting the antenna to the proper rectification circuit. In the case of RF energy harvesting systems, it is important to take into account the radiation characteristics of the antenna, which include its operating frequency, bandwidth, polarization, directivity, gain, and power flux density, in addition to the number of resonant frequencies that the receiving antenna can support. The multiband antennas can be more beneficial from the perspective of RF energy harvesting since they can simultaneously receive RF power from several radio frequency bands that are being delivered by various RF sources from various locations [3, 4]. The researchers have implemented different types of receiving antennas employed by RF energy harvesting devices, including low-profile antennas, multiband antennas, and wideband antennas, for example. Niotaki et al. [5] introduced a slot-loaded dual-band (915 MHz and 2.45 GHz) folded dipole antenna fabricated on an Arlon 25N substrate. Song et al. [6] introduced a bow-tie-shaped planar cross-dipole patch antenna implemented on an FR-4 substrate that supports a frequency range of (550 MHz–2.5 GHz). Furthermore, Shen et al. [7] introduced a dual-port L-probe microstrip patch antenna consisting of two single-port L-probe patch antennas stacked back-to-back with adjacent grounds implemented on a Rogers 3003 substrate that supports three frequency bands with resonating frequencies of 925 MHz, 1.85 GHz, and 2.15 GHz. Also, Roy et al. [8] introduced a dual-plane bow-tie dipole antenna with a triangular shape fabricated on an FR-4 substrate that supports four frequency bands with resonating frequencies of 0.85 GHz, 1.81 GHz, 2.18 GHz, and 2.4 GHz. Also, Meher et al. [17] introduced a circularly polarized low-profile chamfered rectan-

* Corresponding author: Mohammed M. Hasan (mohammed.muataz.eng22@stu.uoninevah.edu.iq).

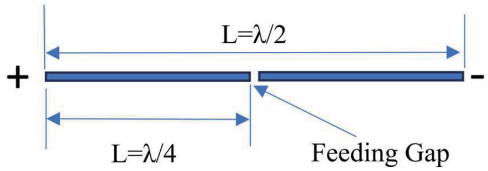

FIGURE 1. Illustration of a conventional half-wave dipole antenna.

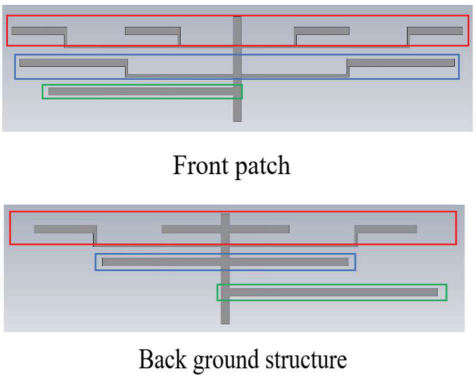

FIGURE 2. The basic design of the proposed antenna (Antenna-1); the upper fins highlighted by red; the middle fins highlighted by blue; the lower fins highlighted by green.

gular dielectric resonator antenna that supports an impedance bandwidth of 2.25 GHz to 3.81 GHz and was implemented using alumina material with a high dielectric constant of 9.9. This paper proposes a multiband microstrip patch antenna (Antenna-1) that supports a tremendous number of eleven resonating frequencies tuned to target the most required frequencies utilized by RFEH systems, including mobile DCS 1800, mobile LTE, mobile 5G WLAN, and WIMAX services. The proposed antenna is simulated with CST Studio software using an FR-4 substrate with a dielectric constant $\varepsilon_r = 4.3$, a thickness of 1.6 mm, and a loss tangent (δ) of 0.025. Furthermore, perfect electrical conductor (PEC) material was selected for creating the front patch and the back ground structure of the proposed antenna with [0.035 mm] of thickness. Also, a time domain solver was selected in the CST software during the simulation of the proposed antenna.

2. DESIGN AND GEOMETRY OF THE PROPOSED ANTENNA-1

2.1. A Brief Review of the Half-Wave Dipole Antenna

The conventional half-wave dipole antenna consists of a liner conductive element usually formed from a thin wire and has a total length of ($L = \lambda/2$) of the target frequency of operation, where (λ) is the wave length of the signal. This type of antenna is typically fed by means of a voltage signal applied across a gap that is introduced halfway along its length. This gap will split the antenna into two poles, and alternating opposite electrical charges will exist at the ends of these two poles, so that when the left end is positively charged, the right end is negatively charged, as shown in Figure 1. This is where the antenna gets the name dipole, meaning "two poles" because of the two electrical charge concentrations existing at either end of the conductor [9].

2.2. Antenna-1 Design and Construction

The proposed multiband patch antenna (Antenna-1) is constructed based on the concepts of the half-wave dipole antenna, since the frequency is inversely proportional to the wavelength of the signal. The first step in designing the proposed antenna was to select three different operating frequencies (0.5 GHz, 0.9 GHz, and 1.8 GHz). Those are the lower ranges of frequencies that may meet the needs for RF energy harvesting applications. The 1.8 GHz frequency is utilized by mobile LTE, mobile DCS, and mobile 5G services; the 0.9 GHz frequency is utilized by mobile LTE and mobile GSM; and the 0.5 GHz frequency is utilized by WiMAX and TV/Radio Broadcasting services. These three frequencies were selected in order to approximately calculate the maximum lengths of the fins that are required for constructing the proposed antenna (Antenna-1). Later on, in the advanced design stages, the proposed Antenna-1 will be copied and scaled down by a specific scale factor, then cascaded to implement the final design of the proposed antenna (Antenna-1). The scale-down process will shorten the length of each of the fins, which may correspond to the quarter wavelength (λ/4) and result in higher resonating frequencies. Figure 2 illustrates the basic design of the proposed multiband (Antenna-1).

Since the proposed antenna (Antenna-1) is designed to be constructed using a thickness of 1.6 mm PCB (Printed Circuit Board) technology on an FR-4 substrate with a dielectric constant [$\varepsilon_r = 4.3$], Equation (1) is used to approximately calculate the values for the maximum lengths of the (Antenna-1) fins [10]. By putting numbers in Equation (1), the operating frequency 0.5 GHz results in a wavelength (λ) equal to [289 mm] and the quarter wavelength (λ/4) equal to [72 mm]. Further, the operating frequency 0.9 GHz results in a wavelength (λ) equal to [160 mm] and the quarter wavelength (λ/4) equal to [40 mm], and the operating frequency 1.8 GHz results in a wavelength (λ) equal to [80 mm] and the quarter wavelength (λ/4) equal to [20 mm].

$$\lambda = \frac{C}{\sqrt{\varepsilon_r} F} \tag{1}$$

where:

C = The speed of light [meter/second].
λ = The maximum operating wavelength [meter].
F = The operating frequency [hertz].
ε_r = Dielectric constant.

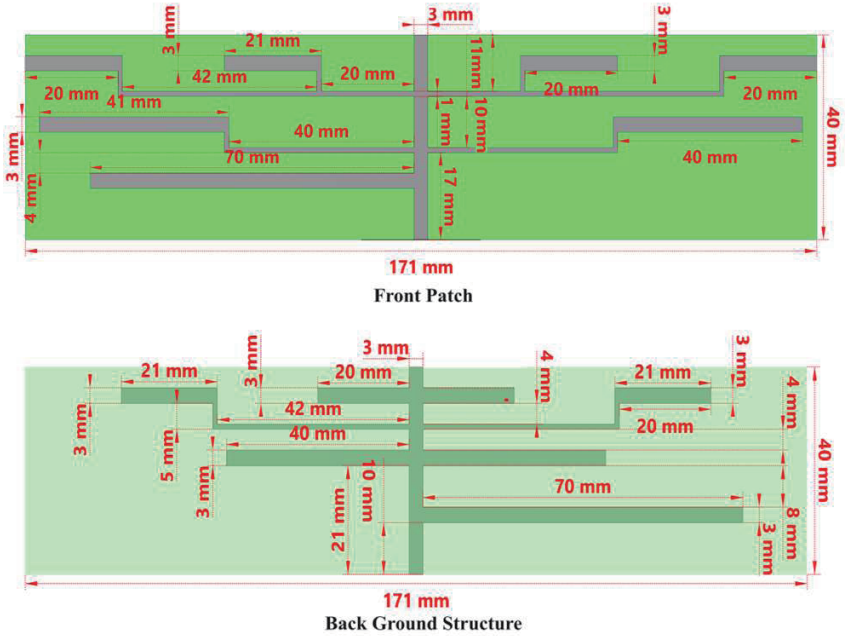

FIGURE 3. The dimensions of the proposed antenna (Antenna-1).

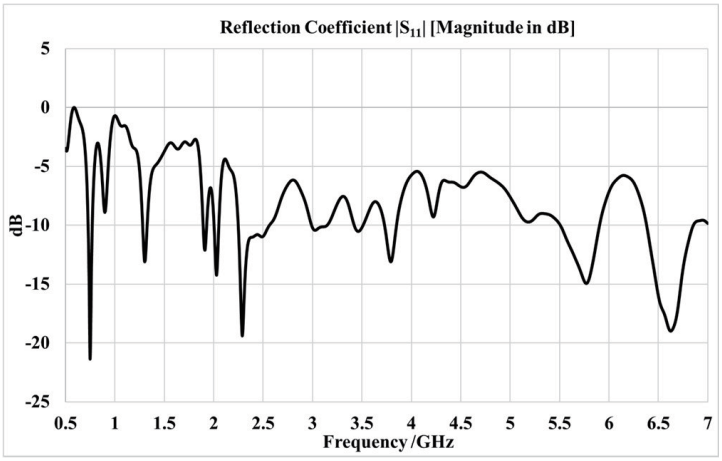

FIGURE 4. The simulated results of the reflection coefficient $|S_{11}|$ for the proposed (Antenna-1).

The front patch of the proposed antenna (Antenna-1) is implemented on a substrate with dimensions of [171 mm] of width and [40 mm] of length. It is started by creating a total of seven (7) fins that are connected with a single vertical microstrip feed line centered on the front patch. The microstrip feed line dimensions were [40 mm] of length, [3 mm] of width, and [0.035 mm] of thickness, respectively. The antenna's lower fins, middle fins, and upper fins were distributed along each side of the vertical microstrip feed line by using four (4) thin horizontal feeding inset lines having the same width of [1 mm] and different lengths, as shown in Figure 3, All seven (7) fins have the same width of [3 mm] and length of [70 mm] for the single lower fin, [40 mm] for the two middle fins, and [20 mm] for the four upper fins, respectively. The back ground structure also has a total of seven (7) fins, and it is constructed similarly to the front patch instead of using only two horizontal feeding insets for the two outer upper fins since the other two upper fins, two middle fins, and one lower fin were directly connected to the centered vertical microstrip feed line of the back ground structure. The widths of all the fins are equal to [3 mm]. The width of the vertical microstrip feed line is the same for the front patch and back ground structure, which is equal to [3 mm], as shown in Figure 3. The lengths of the antenna lower fins, middle fins, and upper fins should approximately correspond to the quarter wavelength ($\lambda/4$) of the three selected operating frequencies as shown in Figure 2. Therefore, from the previous calculation, three different lengths for the proposed Antenna 1 were selected: [70 mm] length for the lower fins, [40 mm] length for the middle fins, and [20 mm] length for the upper fins. Figure 3 shows the dimensions of the basic design of the proposed Antenna 1.

TABLE 1. The simulated results for the basic design of the proposed (Antenna-1).

Resonating Frequency [GHz]	Minimum Frequency [GHz]	Maximum Frequency [GHz]	Bandwidth [GHz]	Reflection Coefficient $\|S_{11}\|$ [dB]
0.747	0.728	0.770	0.042	−21.30
1.300	1.279	1.325	0.046	−13.10
1.910	1.891	1.927	0.036	−12.14
2.027	2.002	2.050	0.048	−14.23
2.287	2.246	2.562	0.316	−19.38
3.022	2.988	3.146	0.158	−10.42
3.46	3.420	3.510	0.090	−10.52
3.789	3.727	3.848	0.121	−13.09
5.771	5.506	5.903	0.397	−14.94
6.623	6.379	6.852	0.473	−19.00

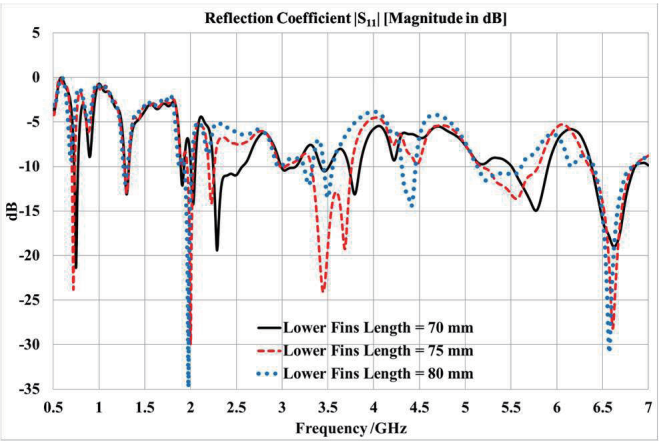

FIGURE 5. The simulated results of the reflection coefficient $|S_{11}|$ for the proposed (Antenna-1) when increasing the length of the lower fins.

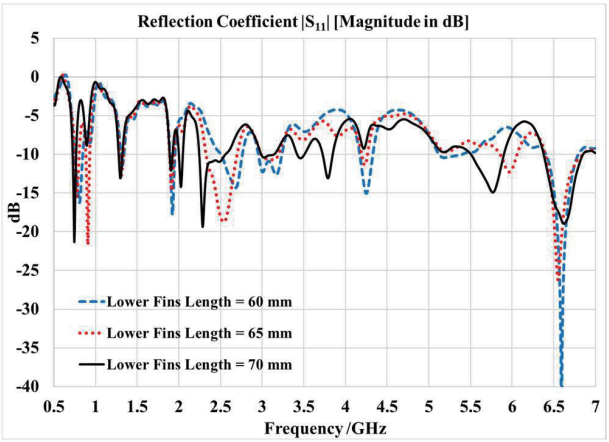

FIGURE 6. The simulated results of the reflection coefficient $|S_{11}|$ for the proposed (Antenna-1) when decreasing the length of the lower fins.

2.3. Simulated Results for the Proposed Antenna-1)

The reflection coefficient $|S_{11}|$ is the main antenna parameter that shows the antenna characteristics and performance for each operating frequency. Figure 4 shows the simulated results of the reflection coefficient $|S_{11}|$ for the proposed antenna (Antenna-1). The results show ten (10) resonating frequencies: (0.747 GHz), (1.300 GHz), (1.910 GHz), (2.027 GHz), (2.287 GHz), (3.022 GHz), (3.46 GHz), (3.789 GHz), (5.771 GHz), and (6.623 GHz). As mentioned previously, Equation (1) was used only to approximately select reasonable lengths for the lower fins, middle fins, and upper fins. The (0.9 GHz) frequency appeared in the frequency spectrum with a reflection coefficient $|S_{11}|$ of [−8.8 dB], so it will be neglected since it has not crossed [−10 dB] in order to be considered a valid operating frequency. For the 1.8 GHz frequency shifted to 1.9 GHz and for the 0.5 GHz frequency shifted to 0.7 GHz, Table 1 shows all the resonating frequencies for the proposed antenna (Antenna-1).

3. PARAMETRIC ANALYSIS FOR THE PROPOSED (ANTENNA-1)

3.1. Impact of Increasing the Length of the Lower Fins

Figure 5 shows the simulated results of the reflection coefficient $|S_{11}|$ when increasing the length of the proposed antenna (Antenna-1) lower fins. The simulated results show that when increasing the length of the lower fins from [70 mm] to [75 mm], the frequency 5.771 GHz shifted left to be 5.55 GHz; the frequency 3.789 GHz shifted left to be 3.45 GHz; and the frequency 2.287 GHz shifted left to be 2.22 GHz on the frequency spectrum. Furthermore, increasing the length of the lower fins from [70 mm] to [80 mm] results in the frequency 5.771 GHz shifted left to be 5.22 GHz; the frequency 3.789 GHz shifted left to be 3.49 GHz; and the frequency 2.287 GHz vanished. The decrease in the resonating frequencies was expected since the frequency is inversely proportional.

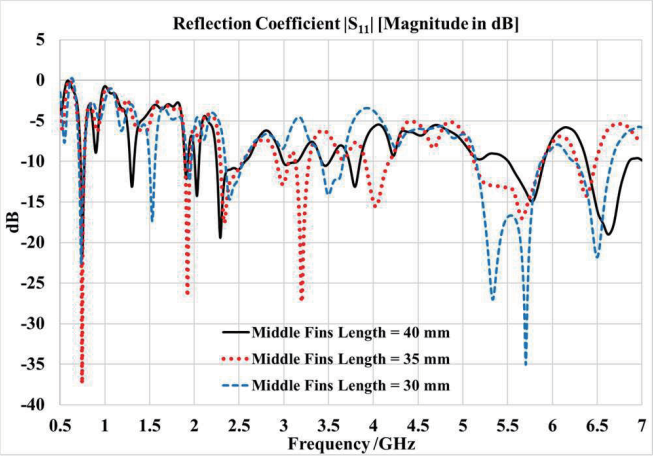

FIGURE 7. The simulated results of the reflection coefficient $|S_{11}|$ for the proposed (Antenna-1) when decreasing the length of the middle fins.

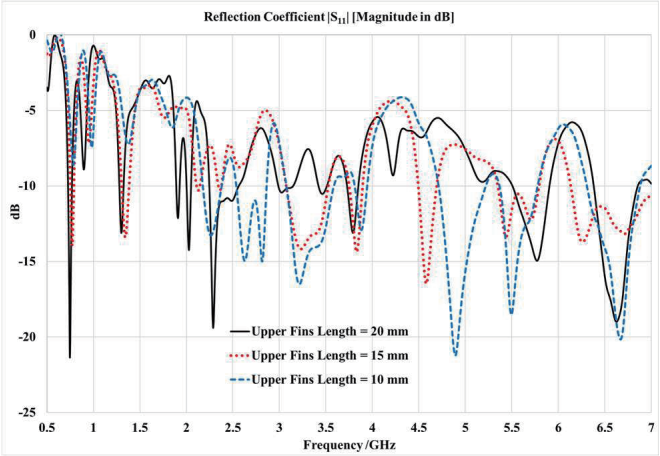

FIGURE 8. The simulated results of the reflection coefficient $|S_{11}|$ for the proposed (Antenna-1) when decreasing the length of the upper fins.

3.2. Impact of Decreasing the Length of the Lower Fins

Figure 6 shows the simulated results of the reflection coefficient $|S_{11}|$ when the length of the proposed antenna (Antenna-1) lower fins is decreased. The simulated results show that when the length of the lower fins is decreased from [70 mm] to [65 mm], the frequency 0.747 GHz shifted right to be 0.9095 GHz; the frequency 2.287 GHz shifted right to be 2.5402 GHz; and the frequency 5.771 GHz shifted right to be 5.9665 GHz on the frequency spectrum. The increase in the resonating frequencies was expected since the frequency is inversely proportional to the wavelength of the signal.

3.3. Impact of Decreasing the Length of the Middle Fins

Figure 7 shows the simulated results of the reflection coefficient $|S_{11}|$ when the length of the proposed antenna (Antenna-1) middle fins is decreased. Since increasing the length of the middle fins of (Antenna-1) will result in overlap between the middle fins of the front patch and the middle fins of the back ground structure, only decreasing the length of the middle fins of (Antenna-1) was studied. The simulated results show that when the length of the middle fins is decreased from [40 mm] to [35 mm], the frequency 1.300 GHz vanished; the frequency 2.287 GHz shifted right to be 2.333 GHz; and the frequency 3.789 GHz shifted right to 4.03 GHz of the frequency spectrum, while a special case appeared for the frequencies 5.771 GHz and 6.623 GHz that were shifted to the left of the frequency spectrum to be 5.66 GHz and 6.37 GHz, respectively. Also, the reflection coefficient $|S_{11}|$ was improved for some of the resonating frequencies with the introduction of a new resonating frequency 3.2 GHz. Furthermore, by decreasing the length of the middle fins from [40 mm] to [30 mm], the frequency 1.300 GHz shifted right to 1.527 GHz, and the frequency 2.287 GHz shifted right to 2.39 GHz of the frequency spectrum, while a special case appeared for the frequencies 3.789 GHz and 6.623 GHz, which were shifted to the left of the frequency spectrum to be 3.49 GHz and 6.49 GHz, respectively, with significant improvements in the bandwidth and the reflection coefficient $|S_{11}|$ for the frequency 5.771 GHz.

3.4. Impact of Decreasing the Length of the Upper Fins

Figure 8 shows the simulated results of the reflection coefficient $|S_{11}|$ when the length of the proposed antenna (Antenna-1) upper fins is decreased. The simulated results show that when the length of the upper fins is decreased from [20 mm] to [10 mm], the frequency 0.747 GHz vanished, and the frequency 1.300 GHz shifted right to be 2.26 GHz; the frequency 1.910 GHz shifted right to 2.62 GHz; the frequency 2.027 GHz shifted right to 2.81 GHz; the frequency 2.287 GHz shifted right to 3.21 GHz; and the frequency 3.789 GHz shifted right to 3.88 GHz of the frequency spectrum, while a special case appeared for the frequencies 5.771 GHz and 6.623 GHz, which were shifted to the left of the frequency spectrum to be 4.89 GHz and 5.49 GHz, respectively, with significant improvements in the bandwidth for the frequency (3.21 GHz) and improvements in the reflection coefficient $|S_{11}|$ for the frequency (4.89 GHz).

3.5. Impact of Changing the Fin Width

Figure 9 shows the simulated results of the reflection coefficient $S_{11}|$ when changing all the fins widths for the proposed antenna (Antenna-1). The simulated results show that when the widths of all (Antenna-1) fins are decreased from [3 mm] to [2 mm], the reflection coefficient $|S_{11}|$ was improved for the frequencies 0.747 GHz, 1.300 GHz, 2.027 GHz, and 2.287 GHz, while diminishing for the frequencies 1.910 GHz and 5.771 GHz. Furthermore, the impact of increasing the width of all (Antenna-1) fins from [3 mm] to [4 mm] results in an improvement in the reflection coefficient $|S_{11}|$ for the frequencies 0.9 GHz, 1.910 GHz, and 6.623 GHz, respectively. The best results for the reflection coefficient $|S_{11}|$ were ob-

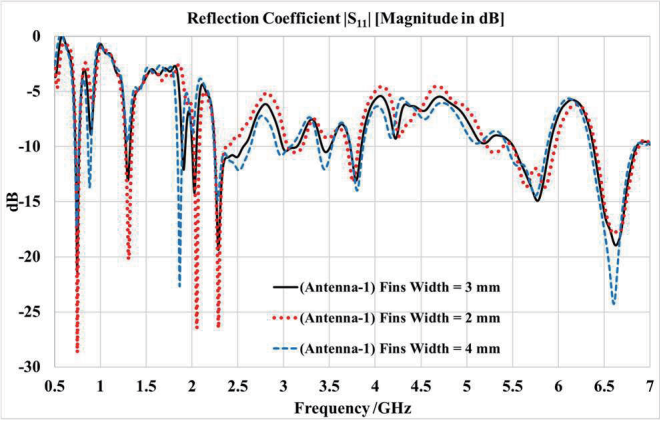

FIGURE 9. The simulated results of the reflection coefficient $|S_{11}|$ when changing all of the fin's width for the proposed (Antenna-1).

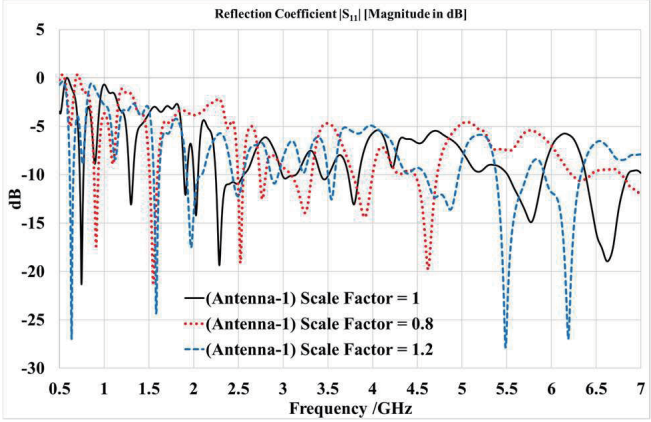

FIGURE 10. The simulated results of the reflection coefficient $|S_{11}|$ when changing the scale of the proposed antenna (Antenna-1).

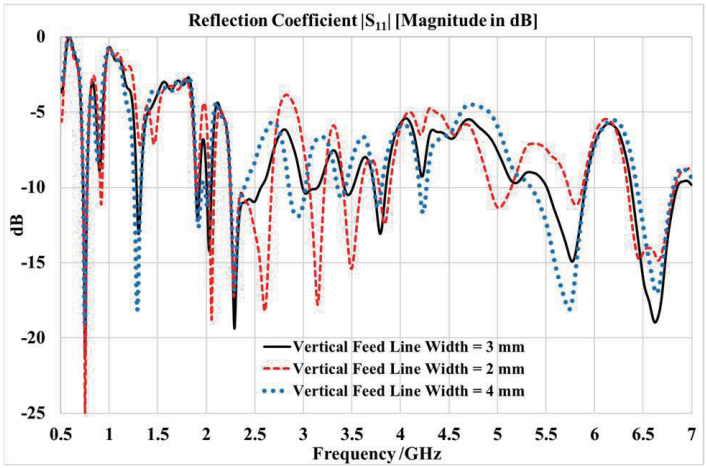

FIGURE 11. The simulated results of the reflection coefficient $|S_{11}|$ when changing the width of the microstrip vertical feed line of the proposed antenna (Antenna-1).

tained when setting the value of all (Antenna-1) fins' widths to [2 mm].

3.6. Impact of Changing the Scale of Antenna-1

Figure 10 shows the simulated results of the reflection coefficient $|S_{11}|$ when the scale of the proposed antenna (Antenna-1) is changed. The simulated results show that scaling down the antenna with a scale factor of (0.8) results in shifting all the resonating frequencies to the right of the frequency spectrum. Also, the two resonating frequencies of 5.771 GHz and 6.623 GHz disappeared since the frequency spectrum studied was from 0.5 GHz to 7 GHz, whereas the impact of scaling up the antenna with a scale factor of (1.2) results in shifting all the resonating frequencies to the left of the frequency spectrum.

3.7. Impact of Changing the Width of the Microstrip Vertical Feed Line

Figure 11 shows the simulated results of the reflection coefficient $|S_{11}|$ when the microstrip vertical feed line width is changed for the proposed antenna (Antenna-1). The simulated results show that when the width of the antenna microstrip vertical feeding line is changed from [3 mm] to [4 mm], the reflection coefficient $|S_{11}|$ is improved for the frequencies 1.300 GHz and 5.771 GHz while diminishing for the frequencies 2.027 GHz and 6.623 GHz, whereas when the width of the antenna microstrip vertical feed line is decreased from [3 mm] to [2 mm], four new frequencies appear in the frequency spectrum, 2.6 GHz, 3.14 GHz, 3.49 GHz, and 5 GHz, respectively. The optimal results for the reflection coefficient $|S_{11}|$ were obtained when setting the width value of the antenna microstrip vertical feed line to [2 mm].

4. ANTENNA-1 OPTIMIZATION

In order to get the best performance from the proposed multiband antenna (Antenna-1) and target the frequencies of interest for RF energy harvesting applications, many modifications were made to the antenna based on the simulated results that were collected from the parametric study of the antenna. The first stage of optimization is obtained by: Firstly, set the antenna microstrip vatical feed line width to [2 mm]. Secondly,

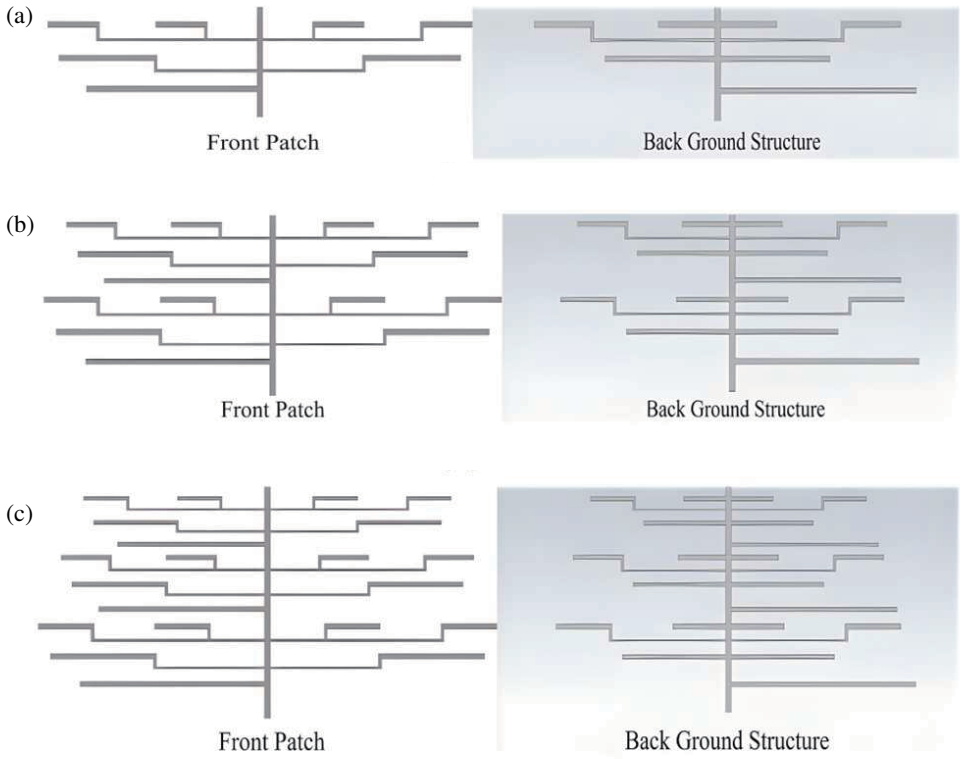

FIGURE 12. The three optimization stages of the proposed antenna: (a) the first stage of optimization (Antenna-1-a); (b) the second stage of optimization (Antenna-1-b); (c) the third stage of optimization (Antenna-1-c).

set the width of all the antenna fins to [2 mm]. Thirdly, set the antenna lower fins length to [68 mm], the middle fins length to [38 mm], and the upper fins length to [19.5 mm], respectively. After the previous modifications, the antenna is named Antenna-1-a, as shown in Figure 12(a). The second stage of optimizing Antenna-1 is implemented by copying and scaling down Antenna-1-a using a scale factor of 0.9 and attaching it to the top of Antenna-1-a. This will create Antenna-1-b, which is the second stage of optimizing the antenna, as shown in Figure 12(b). The third stage of optimizing Antenna-1 was implemented by scaling down Antenna-1-a using a scale factor of 0.8 and attaching it on top of Antenna-1-b then scaling up the resultant antenna using a scale factor of 1.01. This will create the final design (Antenna-1-c), as shown in Figure 12(c). The previous cascaded design procedure was implemented in order to get a wide variety of lengths for the antenna fins that target many frequencies required for RF energy harvesting applications. Figure 13 shows the dimensions of Antenna-1-c which is the final design, the proposed antenna (Antenna-1).

Furthermore, Figure 14 shows the simulated results of the reflection coefficient $|S_{11}|$ for each optimization stage (Antenna-1-a), (Antenna-1-b), and (Antenna-1-c). The simulated results show major improvements in performance for the third optimization stage (Antenna-1-c), whereas the simulated results for the first stage optimization (Antenna-1-a) show low performance for the frequency band of 5 GHz. Also, the simulated results for the second stage of the optimization (Antenna-1-b) show low performance for the frequency bands (2.4 GHz and 1.8 GHz). Therefore, the third stage of optimization (Antenna-1-c) is the optimal stage for A ntenna-1, and it is the final design for the proposed antenna (Antenna-1). Table 2 shows the simulated results for the final design of the proposed antenna (Antenna-1-c).

5. RESULTS AND DISCUSSION

The multiband antenna (Antenna-1) was designed carefully and studied step-by-step in order to target the most required frequencies for RF energy harvesting applications. The simulated results for the final design of the proposed antenna (Antenna-1-c) showed outstanding performance. Since the antenna supports a high number of total (11) eleven resonating frequencies, as shown in Table 2, all of them are required for RF energy harvesting applications. Furthermore, the proposed antenna (Antenna-1-c) covered all of the frequencies utilized by the 2.4 GHz (IEEE 802.11) band, which is the most popular and widely used by WLAN services, as well as all of the downlink frequencies utilized by the mobile DCS 1800 frequency band (1,805 MHz–1,880 MHz) and all of the downlink frequencies for the band 68 (753 MHz–783 MHz) that are utilized by the mobile LTE/5G in Europe, the Middle East, and Africa. Furthermore, the final design of the proposed antenna (Antenna-1-c) has achieved a high gain for most of its resonating frequencies. For example, the antenna achieved a high gain of 4.49 dBi at the frequency of 2.4527 GHz, and a peak gain of 6.349 dBi at the frequency of 3.95 GHz. Also, the simulated results of the proposed multiband antenna (Antenna-1-c) showed a high

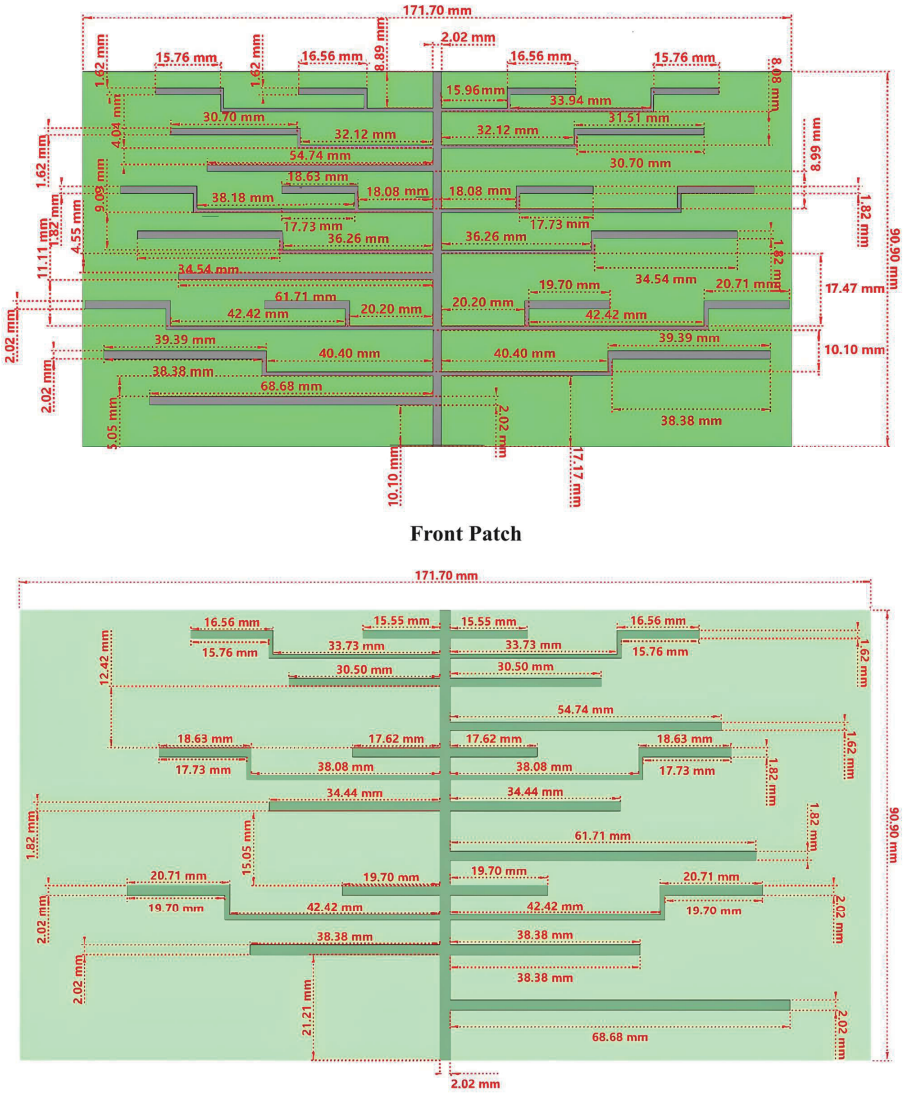

FIGURE 13. The dimensions of the final design of the proposed antenna (Antenna-1-c).

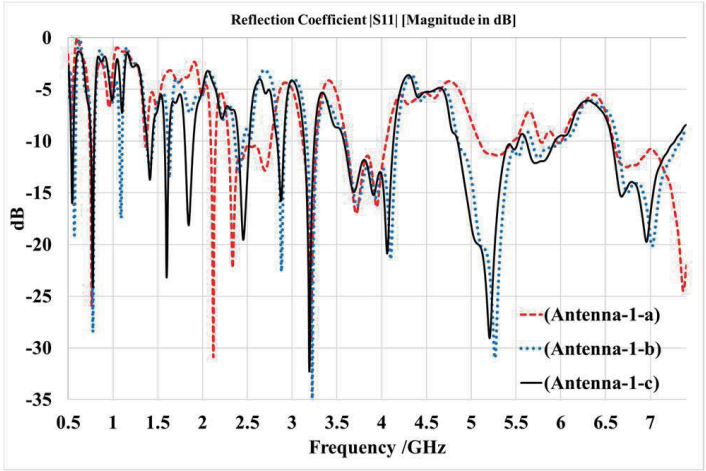

FIGURE 14. The simulated results of the reflection coefficient $|S_{11}|$ for each optimization stage (Antenna-1-a), (Antenna-1-b), and (Antenna-1-c).

TABLE 2. Simulated results for the final design of the proposed antenna (Antenna-1-c).

Resonating Frequency (GHz)	Return Loss $\lvert S_{11}\rvert$ (dB)	Minimum Frequency (GHz)	Maximum Frequency (GHz)	Band width (GHz)	Directivity (dBi)	Peak Gain	Applications	Reference
0.776	−24	0.75109	0.7892	0.03811	5.064	2.919 dBi @0.7892 GHz	WIMAX, Mobile LTE, Mobile 5G	[11, 12]
1.4108	−13.73	1.38	1.4382	0.0582	2.367	0.7028 dBi @1.4382 GH	WIMAX, Mobile LTE, Mobile 5G	[11, 12]
1.5971	−23.1	1.5757	1.6269	0.0512	4.151	1.572 dBi @1.6269 GHz	Mobile LTE, Mobile 5	[11, 12]
1.8455	−18.13	1.8014	1.8973	0.0959	4.734	1.433 dBi @1.8455 GHz	Mobile 5G, Mobile LTE, Mobile DCS 1800	[11, 12]
2.4527	−19.53	2.3989	2.521	0.1221	6.267	4.49 dBi @2.4527 GH	WLAN, WIMAX, Mobile LTE, Mobile 5G	[11, 12]
2.8736	−15.75	2.8305	2.9087	0.0782	6.106	2.989 dBi @ 2.8305 GHz	WIMA	[11, 12]
3.191	−32.18	3.133	3.24813	0.11513	4.889	3.371 dBi @3.133 GH	RADIOLOCATION, Active sensors (satellite	[11, 12]
4.06	−20.86	3.57795	4.13119	0.55324	8.371	6.349 dBi @3.95 GHz	Mobile LTE, WLAN, WIMAX, Mobile 5G	[11, 12]
5.2058	−29.05	4.8481	5.5255	0.6774	7.571	5.486 dBi @ 5.33 GHz	WLAN, WIMAX, Mobile LTE, Mobile 5G	[11, 12]
5.7164	−12.12	5.615	5.9333	0.3183	6.236	4.921 dBi @5.615 GH	WLAN, WIMAX, Mobile LTE, Mobile 5G	[11, 12]
6.9584	−19.74	6.5738	7.2734	0.6996	8.495	5.386 dBi @ 6.9584 GHz	WLAN, Mobile LTE, Mobile 5	[11, 12]

bandwidth capacity for most of its resonating frequencies, making it a perfect antenna for radio frequency energy harvesting applications. For example, the antennas have a bandwidth capacity of 677 MHz at the resonating frequency of 5.2 GHz, which covers a lot of frequencies utilized by WLAN, WIMAX, and mobile LTE services. Figure 15 shows the simulated 3D radiation pattern of the directivity magnitude in dBi for some of the proposed multiband (Antenna-1-c) supported frequencies. Also, Figure 16 shows the simulated 2D radiation pattern. The simulated results for the 3D radiation pattern of the directivity showed that the proposed antenna has omnidirectional radiation characteristics for the resonating frequency 1.4108 GHz, which is utilized by WIMAX, Mobile LTE, and Mobile 5G services.

The results show that the proposed antenna has major performance improvements compared to other proposed works shown in Table 3. Since the proposed antenna (Antenna-1-c) supports more resonating frequencies, it is expected to cover more wireless services required for RFEH applications. Furthermore, the proposed antenna (Antenna-1-c) achieved a high gain for most of its operating frequencies compared to its size and thickness since it is much thinner than [5, 7, 13, 14] and smaller than [6, 8, 15]. It also needs to be mentioned that an FR-4 substrate is much cheaper than (Arlon 25N) and (Rogers 3003) substrates, and the gain is directly proportional to antenna physical size and thickness [16]. Figure 17 shows the simulated results of the antenna gain versus frequency.

TABLE 3. Evaluation of the proposed work in comparison to previous works.

Reference	Antenna Size [cm^3]	Substrate Type	Operating Frequency	Peak Gain [dBi]
[5]	60 mm×60 mm×60 mm	Arlon 25N	915 MHz, 2.45 GHz	1.87 dBi@915 GHz, 4.18 dBi@2.45
[6]	160 mm×160 mm×1.6 mm	FR-4	550 MHz–2.5 GHz (Wideband)	5 dBi@ 2.15 GHz
[7]	200 mm×175 mm×46.6 mm	Rogers 3003	925 MHz, 1.85 GHz, and 2.15 GHz	8.15 dBi @915 MHz, 7.15 dBi@1.850 GHz, 8.15 dBi@2.15 GHz
[13]	120 mm×120 mm×30 mm	FR-4	2.1 GHz, (2.4 GHz–2.48 GHz), (3.3 GHz–3.8 GHz)	7 dBi@2 GHz, 5.5 dBi@2.5 GHz, 9.2 dBi@3.5 GHz
[14]	100 mm×100 mm×5 mm	FR-4	2.4 GHz	8.36
[8]	160 mm×160 mm×1.6 mm	FR-4	0.85 GHz, 1.81 GHz, 2.18 GHz, 2.4 GHz	3.95 dBi@0.85 GHz, 4.45 dBi@1.81 GHz, 4.42 dBi@2.18 GHz, 4.82 dBi@2.4 GHz
[15]	160 mm×160 mm×1.6 mm	FR-4	0.9 GHz, 1.8 GHz, 2.12 GHz, and 2.4 GHz	Peak gain of 6 dBi
Proposed work	171.7 mm×90.9 mm×1.6 mm	FR-4	0.776 GHz, 1.4108 GHz, 1.5971GHz, 1.8455 GHz, 2.4527 GHz, 2.8736 GHz, 3.191 GHz, 4.06 GHz, 5.2058 GHz, 5.7164 GHz, 6.9584 GHz	2.919 dBi@0.7892 GHz 0.7028 dBi@1.4382 GHz 1.572 dBi@1.6269 GHz 1.433 dBi@1.8455 GHz 4.49 dBi@2.4527 GHz 2.989 dBi@2.8305 GHz 3.371 dBi@3.133 GHz 6.349 dBi@3.95 GHz 5.486 dBi@5.33 GHz 4.921 dBi@5.615 GHz 5.386 dBi@6.9584 GHz

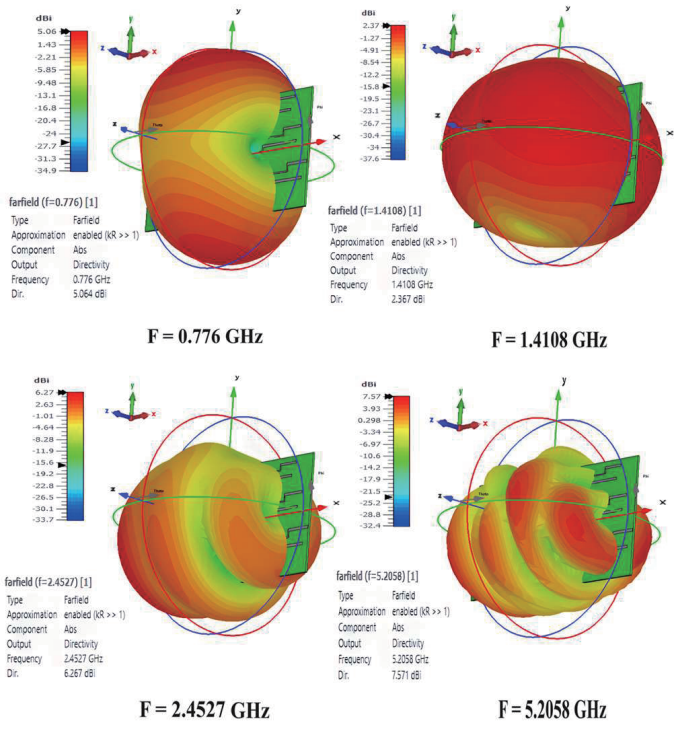

FIGURE 15. The simulated 3D radiation pattern of the directivity magnitude in [dBi] for some of (Antenna-1-c) supported frequencies.

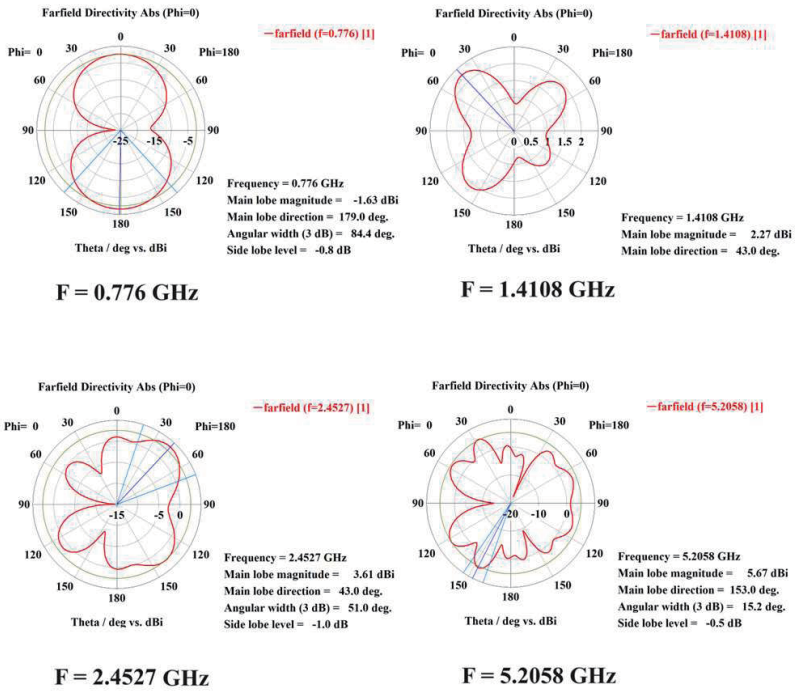

FIGURE 16. The simulated 2D radiation pattern of the directivity magnitude in [dBi] for some of (Antenna-1-c) supported frequencies.

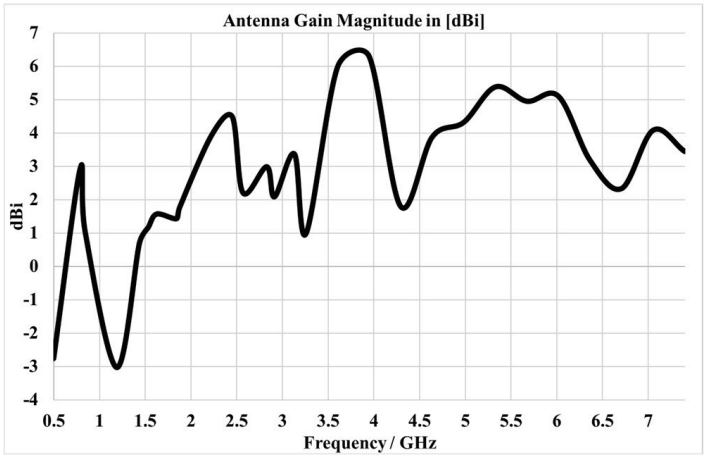

FIGURE 17. The simulated results of the antenna gain versus frequency for the proposed optimized antenna (Antenna-1-c).

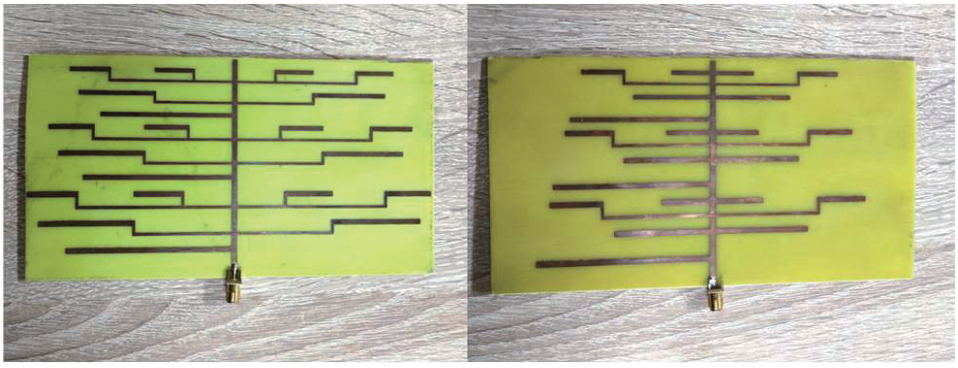

FIGURE 18. The physical structure of the proposed optimized antenna (Antenna-1-c).

FIGURE 19. The testing environment used to measure the normalized 2D radiation pattern for the proposed antenna (Antenna-1-c).

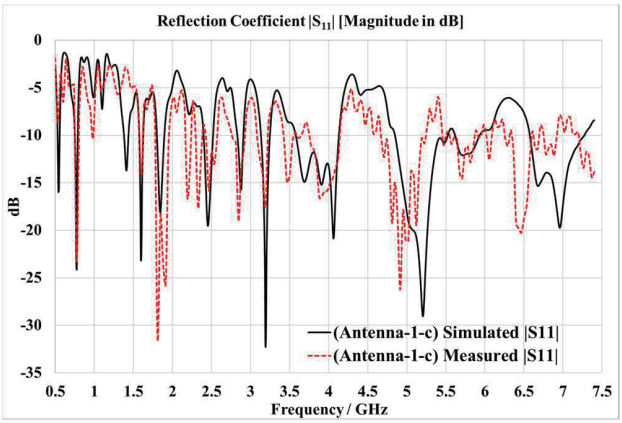

FIGURE 20. The reflection coefficient $|S_{11}|$ for both the simulated and the practical manufactured (Antenna-1-c).

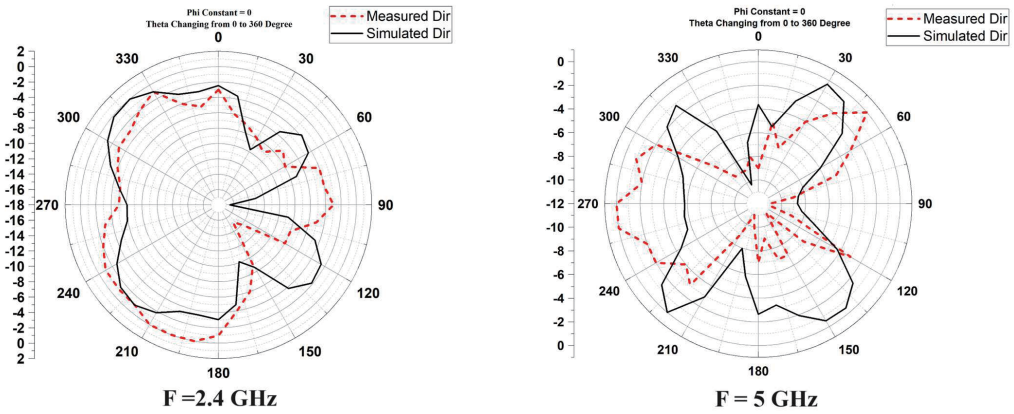

FIGURE 21. The normalized 2D radiational pattern of the directivity for the proposed antenna (Antenna-1-c) showed the simulated and measured results.

6. EXPERIMENTAL RESULTS

The proposed multiband antenna (Antenna-1-c) was manufactured using PCB technology on an FR-4 substrate, as shown in Figure 18. Figure 19 shows the testing environment and experimental setup. Figure 20 illustrates the comparison results of the reflection coefficient $|S_{11}|$ magnitude in dB between the simulated and manufactured optimized antennas (Antenna-1-c). In addition, Figure 21 illustrates a comparison result of the normalized 2D radiation pattern between the simulated and practical optimized antennas (Antenna-1-c). The experimental results of the practical fabricated antenna were obtained using a similar antenna that acted as a transmitted antenna and was supplied with an input power of 7 dBm and placed line of sight from the proposed receiving antenna at a distance of 83 cm.

The measurement results of the normalized 2D radiation pattern showed good matching for the frequency of 2.4 GHz, and

there was a shift of 30 degrees clockwise compared with the simulated results as shown in Figure 21. The measurement results of the normalized 2D radiation pattern showed better matching with the simulated ones for the frequency of 2.4 GHz compared to the frequency of 5 GHz. This may be because of the difficulties in fabricating antenna, such as the fine details of antenna geometries, soldering effects, and the absence of a completely anechoic laboratory in the university since the measurement was done on a semi-anechoic chamber.

7. CONCLUSION

This paper presents a microstrip patch antenna (Antenna-1) that is designed and tuned carefully in order to target the required frequencies utilized by radio frequency energy harvesting applications. The proposed antenna is simulated with CST Studio Suite software, and then the final design, i.e., Antenna-1-c, is manufactured on an FR-4 substrate with 1.6 mm of thickness. The results showed that the proposed multiband antenna supports a total of eleven (11) resonating frequencies that are utilized by a large number of wireless services, including mobile DCS1800, mobile LTE, mobile 5G, WIMAX, and WLAN services, and all of them are useful for radio frequency energy harvesting applications. Parametric analysis procedures were implemented in the basic design of the proposed antenna, and many modifications were applied in order to optimize the antenna. The optimization process done in three stages in order to reach the final design, i.e., Antenna-1-c. The simulated results showed that the proposed optimized antenna (Anteanna-1-c) achieved a high gain and a high frequency bandwidth for most of its operating frequencies, with a peak gain of 6.349 dBi making it a perfect antenna for radio frequency energy harvesting applications. An evaluation of the proposed work in comparison to previous works showed major performance improvements in terms of antenna thickness, size, gain, and the number of operating frequencies that support a variety of wireless services. Additionally, the measurement results of the normalized 2D radiation pattern and the reflection coefficient $|S_{11}|$ exhibited acceptable tolerance errors compared with the simulated results, considering the challenges of antenna fabrication, including the fine details of antenna geometries, soldering effects, and lack of a fully anechoic chamber at the university where the measurement was made.

REFERENCES

[1] Ullah, M. A., R. Keshavarz, M. Abolhasan, J. Lipman, K. P. Esselle, and N. Shariati, "A review on antenna technologies for ambient RF energy harvesting and wireless power transfer: Designs, challenges and applications," *IEEE Access*, Vol. 10, 17 231–17 267, 2022.

[2] Mouapi, A., "Radiofrequency energy harvesting systems for Internet of Things applications: A comprehensive overview of design issues," *Sensors*, Vol. 22, No. 21, 8088, Nov. 2022.

[3] Rizzoli, V., A. Costanzo, D. Masotti, and F. Donzelli, "Integration of numerical and field-theoretical techniques in the design of single- and multi-band rectennas for micro-power generation," *International Journal of Microwave and Wireless Technologies*, Vol. 2, No. 3-4, 293–303, Aug. 2010.

[4] Divakaran, S. K., D. D. Krishna, and Nasimuddin, "RF energy harvesting systems: An overview and design issues," *International Journal of RF and Microwave Computer-Aided Engineering*, Vol. 29, No. 1, e21633, Jan. 2019.

[5] Niotaki, K., S. Kim, S. Jeong, A. Collado, A. Georgiadis, and M. M. Tentzeris, "A compact dual-band rectenna using slot-loaded dual band folded dipole antenna," *IEEE Antennas and Wireless Propagation Letters*, Vol. 12, 1634–1637, 2013.

[6] Song, C., Y. Huang, P. Carter, J. Zhou, S. Yuan, Q. Xu, and M. Kod, "A novel six-band dual CP rectenna using improved impedance matching technique for ambient RF energy harvesting," *IEEE Transactions on Antennas and Propagation*, Vol. 64, No. 7, 3160–3171, Jul. 2016.

[7] Shen, S., C.-Y. Chiu, and R. D. Murch, "A dual-port triple-band l-probe microstrip patch rectenna for ambient rf energy harvesting," *IEEE Antennas and Wireless Propagation Letters*, Vol. 16, 3071–3074, Oct. 2017.

[8] Roy, S., J. J. Tiang, M. B. Roslee, M. T. Ahmed, A. Z. Kouzani, and M. A. P. Mahmud, "Quad-band rectenna for ambient radio frequency (RF) energy harvesting," *Sensors*, Vol. 21, No. 23, 7838, Dec. 2021.

[9] Khan, A. Q., M. Riaz, and A. Bilal, "Various types of antenna with respect to their applications: A review," *International Journal of Multidisciplinary Sciences and Engineering*, Vol. 7, No. 3, 1–8, 2016.

[10] Ulaby, F. T. and U. Ravaioli, *Fundamentals of Applied Electromagnetics*, Pearson Upper Saddle River, NJ, Jan. 2015.

[11] "Frequency allocation chart for LTE, WiMAX and WLAN systems/bands," Available: https://wireless-instruments.com/lte-wimax-bands/, Jan. 2024.

[12] "The european table of frequency allocations and applications in the frequency range 8.3 kHz to 3000 GHz (ECA TABLE)," Report25 Approved October 2021, Editorial update 7 July 2023.

[13] Chandravanshi, S., S. S. Sarma, and M. J. Akhtar, "Design of triple band differential rectenna for RF energy harvesting," *IEEE Transactions on Antennas and Propagation*, Vol. 66, No. 6, 2716–2726, Jun. 2018.

[14] Said, M. A. M., Z. Zakaria, M. N. Husain, M. H. Misran, and F. S. M. Noor, "2.45 GHz rectenna with high gain for RF energy harvesting," *Telkomnika (Telecommunication Computing Electronics and Control)*, Vol. 17, No. 1, 384–391, Feb. 2019.

[15] Roy, S., J.-J. Tiang, M. B. Roslee, M. T. Ahmed, A. Z. Kouzani, and M. A. P. Mahmud, "Design of a highly efficient wideband multi-frequency ambient RF energy harvester," *Sensors*, Vol. 22, No. 2, 424, Jan. 2022.

[16] Balanis, C. A., *Antenna Theory: Analysis and Design*, John Wiley & Sons, Feb. 2016.

[17] Meher, P. R., S. K. Mishra, and M. A. Halimi, "A low-profile compact broadband CP DRA for RF energy harvesting applications," *IETE Journal of Research*, 1–9, Jul. 2023.